Signal Processing 132 (2017) 221–226

Contents lists available at ScienceDirect

Signal Processing

journal homepage: www.elsevier.com/locate/sigpro

Characterisation of a ground penetrating radar antenna in lossless homogeneous and lossy heterogeneous environments

Craig Warren *, Antonios Giannopoulos

Institute for Infrastructure and Environment, School of Engineering, University of Edinburgh, Edinburgh, Scotland, UK

ARTICLE INFO

Article history:
Received 2 February 2016
Received in revised form
31 March 2016
Accepted 21 April 2016
Available online 23 April 2016

Keywords:
Ultra-wideband antennas
Antenna radiation patterns
Finite-Difference Time-Domain
Ground Penetrating Radar
Modeling
Simulation

ABSTRACT

Directly measuring the radiation characteristics of Ground Penetrating Radar (GPR) antennas in environments typically encountered in GPR surveys, presents many practical difficulties. However it is very important to understand how energy is being transmitted and received by the antenna, especially for areas of research such as antenna design, signal processing, and inversion methodologies. To overcome the difficulties of experimental measurements, we used an advanced modelling toolset to simulate detailed three-dimensional Finite-Difference Time-Domain (FDTD) models of GPR antennas in realistic environments. A semi-empirical soil model was utilised, which relates the relative permittivity of the soil to the bulk density, sand particle density, sand fraction, clay fraction and volumetric fraction of water. The radiated energy from the antenna was studied in lossless homogeneous dielectrics as well as, for the first time, in lossy heterogeneous environments. Significant variations in the magnitude and pattern shape were observed between the lossless homogeneous and lossy heterogeneous environments. Also, despite clear differences in time domain responses from simulations that included only an infinitesimal dipole source model and those that used the full antenna model, there were strong similarities in the radiated energy distributions.

1. Introduction

The diversity of Ground Penetrating Radar (GPR) usage means there are a variety of different GPR systems and antennas. Understanding how energy is transmitted and received by a particular GPR antenna can be beneficial for antenna design and usage, and can improve signal processing techniques like migration and inversion. For example, to achieve accurate amplitude migration of GPR data knowledge of the radiation pattern of the antenna is generally required [1]. The radiation characteristics of any antenna are usually investigated by analysing parameters such as impedance, field pattern shape, and directivity in free space. Crucially, however, for GPR antennas these characteristics must be studied in the different environments that can be encountered in GPR surveys. This is because a complex series of interactions occur between the antenna and the environment, which change how the antenna behaves.

Radiation pattern measurements in free space of simple antennas, as well as for more widely used commercial GPR antennas, have been made [2–4]. There have also been laboratory measurements of radiation patterns of simple antennas over homogeneous materials obtained directly with another antenna [5], and indirectly through the recording of responses from a simple target [4,6]. Received energy patterns were measured from a commercial GPR antenna in a series of oil-in-water emulsions which represented lossy homogeneous environments [7]. However, measuring antenna radiation patterns in lossy heterogeneous environments that are realistic for GPR presents many practical difficulties. This has prompted researchers to develop numerical simulations of GPR antenna radiation patterns.

Simple and more complex antennas have been modelled in free space, and simple antennas have been modelled in realistic environments, but there have been very limited studies that combine realistic GPR antenna models with realistic environments. Models of antennas over layered media have been developed for an off-ground horn antenna using linear transfer functions [8] and for an antenna operating in the near-field using equivalent sets of infinitesimal electric dipoles [9]. The energy distribution of a shielded dipole antenna over various lossless half-spaces was studied by [10], and similarly [7] used an FDTD antenna model to compare simulated and measured data.

This paper presents an investigation of the radiation characteristics of a high-frequency GPR antenna in lossless homogeneous and, for the first time, in lossy heterogeneous environments using detailed FDTD models. An advanced simulation

* Corresponding author.
E-mail addresses: Craig.Warren@ed.ac.uk (C. Warren), A.Giannopoulos@ed.ac.uk (A. Giannopoulos).

http://dx.doi.org/10.1016/j.sigpro.2016.04.010

toolset allowed a detailed model of a GPR antenna to be used in heterogeneous environments that simulate realistic soils. Section 2 describes the development of the FDTD models of the antenna and the soil. The results of the simulations in lossless dielectrics and lossy heterogeneous environments are presented in Section 3. Different values of dielectric constant, and different types and distributions of realistic soil properties are compared. Principal electric and magnetic field patterns are analysed at a range of observation distances from the antenna using a total energy metric.

2. Finite-Difference Time-Domain simulations

All of the simulations conducted for this research used gprMax (http://www.gprmax.com) which is an electromagnetic wave simulator based on the Finite-Difference Time-Domain (FDTD) method. gprMax was originally developed in 1996 [11] and over the past 20 years has been one of the most widely used simulation tools in the GPR community. It has been successfully used for a diverse range of applications in academia and industry [12–17], and has been cited more than 200 times since 2005 [18]. gprMax has recently undergone significant modernisations to the code and also added a number of new advanced features including an unsplit implementation of higher order perfectly matched layers (PMLs) using a recursive integration approach; uniaxially anisotropic materials; dispersive media using multiple Debye, Drude or Lorenz expressions; improved soil modelling using a semi-empirical formulation for dielectric properties and fractals for geometric characteristics; rough surface generation; and the ability to embed complex transducers and targets [19].

2.1. Antenna model

The simulations included a model of a GPR antenna that is representative of a Geophysical Survey Systems, Inc. (GSSI) 1.5 GHz antenna, which is a high-frequency, ground-coupled antenna. The antenna model includes all of the main features and geometry of the real antenna. Details of the antenna model development and initial validation can be found in [20]. A spatial discretisation of $\Delta x = \Delta y = \Delta z =$ 1 mm was chosen as a good compromise between accuracy and computational resources. The Courant Friedrichs Lewy (CFL) condition was enforced which resulted in a time-step of $\Delta t = 1.926$ ps.

2.2. Lossy heterogeneous soil models

gprMax was used to build lossy heterogeneous environments that represent soils with more realistic dielectric and geometrical properties. A semi-empirical model, initially suggested by [21], was used to describe the dielectric properties of the soil. The model relates the relative permittivity of the soil to bulk density, sand particle density, sand fraction, clay fraction and water volumetric fraction. Using this approach, a more realistic soil with a stochastic distribution of the aforementioned parameters can be modelled. The real and imaginary parts of this semi-empirical model can be approximated using a multi-pole Debye function plus a conductive term. This dispersive behaviour has been implemented in gprMax by using a recursive convolution method to express dispersive properties as apparent current density sources [22]. Fig. 1 shows the FDTD mesh of the antenna model on a heterogeneous soil model with a stochastic distribution of realistic dielectric and geometrical properties. The size of each simulation was approximately 385 million cells (28 GB RAM), which required up to 10 h to run (depending on the necessary length of time window) on a 4 GHz Intel Core i7 CPU.

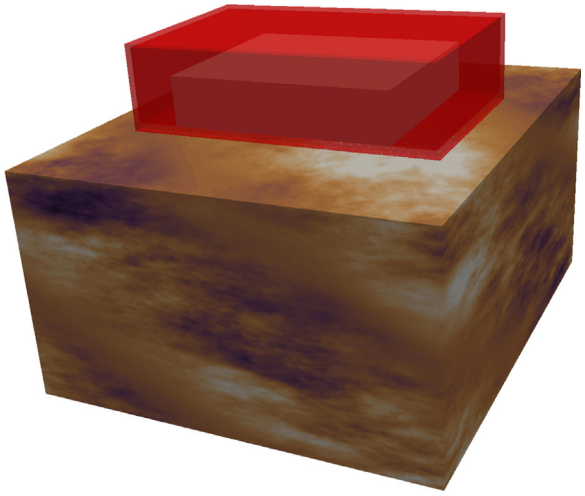

Fig. 1. Antenna (representative of a GSSI 1.5 GHz antenna) and heterogeneous soil model with a stochastic distribution of the volumetric water fraction.

3. Simulated radiation patterns

Traditionally antenna patterns are plotted at a specific single frequency, however these are of limited use in analysing the overall performance of an ultra-wideband (UWB) GPR antenna, e.g. peaks and troughs present in a pattern at a single frequency can interfere constructively and destructively with those present at another frequency. Therefore, a measure of the total energy given by Eq. (1), adapted from [10], was used:

$$\Psi(r, \theta) = \sum_{t=0}^{T} E(r, \theta)^2 \tag{1}$$

Ψ is the total energy at a specific radius (r) and angle (θ); the summation is made over the duration of the time-domain response; and E is the electric field value at a specific radius (r) and angle (θ).

A total of six different environments were investigated:

- Lossless dielectric, relative permittivity $\epsilon_r = 5$.
- Lossless dielectric, relative permittivity $\epsilon_r = 20$.
- Lossy heterogeneous environment with soil properties – sand fraction $S=0.5$, clay fraction $C=0.5$, bulk density $\rho_b = 2$ g/cm^3, and sand particle density $\rho_s = 2.66$ g/cm^3 – and fractal dimension $D=1.5$.
- Lossy heterogeneous environment with soil properties – sand fraction $S=0.5$, clay fraction $C=0.5$, bulk density $\rho_b = 2$ g/cm^3, and sand particle density $\rho_s = 2.66$ g/cm^3 – and fractal dimension $D=2$.
- Lossy heterogeneous environment with soil properties – sand fraction $S=0.9$, clay fraction $C=0.1$, bulk density $\rho_b = 2$ g/cm^3, and sand particle density $\rho_s = 2.66$ g/cm^3 – and fractal dimension $D=2$.
- Lossy heterogeneous environment with soil properties – sand fraction $S=0.1$, clay fraction $C=0.9$, bulk density $\rho_b = 2$ g/cm^3, and sand particle density $\rho_s = 2.66$ g/cm^3 – and fractal dimension $D=2$.

The fractal dimension is a value for characterising fractal patterns or sets by quantifying their complexity.

All the heterogeneous environments had a volumetric water content range of 0.001–0.25, with 50 different materials created in the model to simulate this range. The heterogeneous environments were simulated using a semi-empirical model, initially suggested by [21], to describe the dielectric properties of the soil.

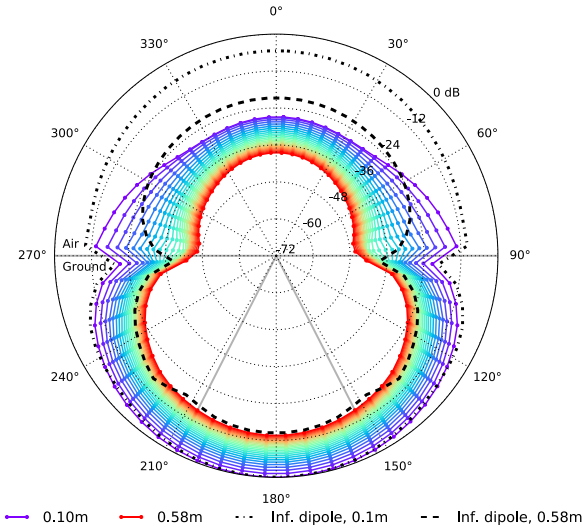

(a) E-plane

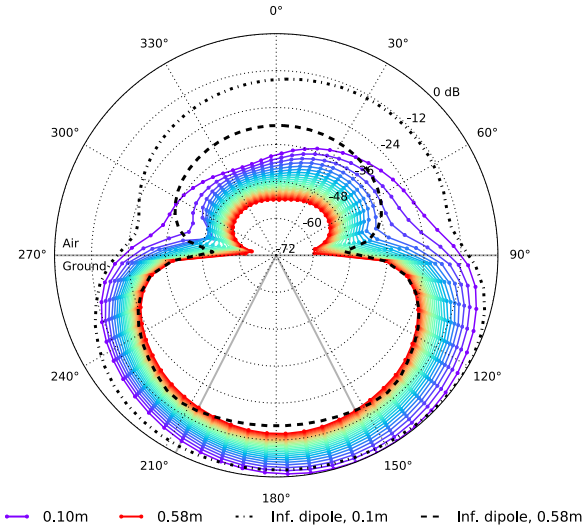

(b) H-plane

Fig. 2. Series of energy patterns from the full antenna model over a dielectric half-space, $\epsilon_r = 5$. Observation distances 0.10–0.58 m at intervals of 0.02 m. Infinitesimal dipole model over a dielectric half-space, $\epsilon_r = 5$ at an observation distances of 0.1 m and 0.58 m.

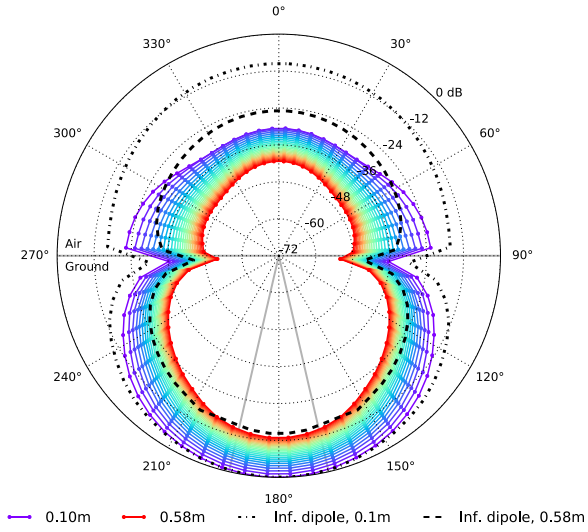

(a) E-plane

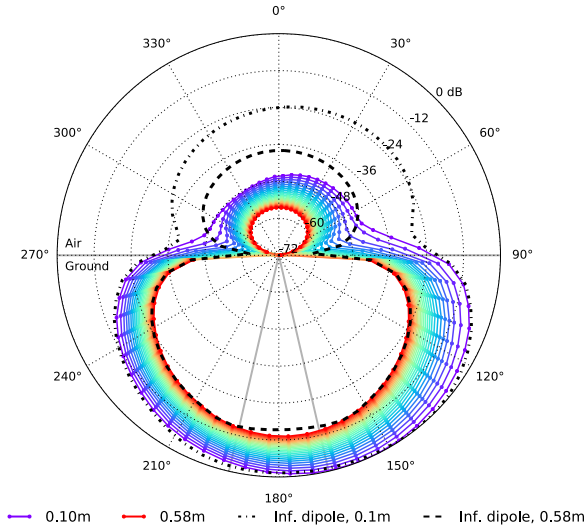

(b) H-plane

Fig. 3. Series of energy patterns from the full antenna model over a dielectric half-space, $\epsilon_r = 20$. Observation distances 0.10–0.58 m at intervals of 0.02 m. Infinitesimal dipole model over a dielectric half-space, $\epsilon_r = 20$ at an observation distances of 0.1 m and 0.58 m.

There are other mixing models, such as the complex refractive index model (CRIM) and the Bruggeman–Hanai–Sen (BHS) model which can also be used to describe heterogeneous mixtures of materials.

Radiation patterns in all the environments were calculated every 0.02 m from a distance of 0.10 m to 0.58 m. The maximum distance was limited by the computational resources available at the time but in any case, as the antenna has a high centre frequency (1.5 GHz) and is ground-coupled, most targets will be detected within a distance of 0.5 m from the antenna.

All patterns are plotted on a logarithmic scale ($10\ \log_{10} \Psi$), and each set of patterns, i.e. the full antenna models and the infinitesimal dipole models (where used), have been normalised according to the maximum value present in the set. Solid grey lines represent the boundary between air and the ground, and are also used to indicate the critical angle window for the lossless dielectric half-spaces.

Figs. 2 and 3 present the principal E- and H-plane patterns in lossless dielectric environments of relative permittivity $\epsilon_r = 5$ and $\epsilon_r = 20$. As expected all of the patterns show a broad main lobe, i.e. there are no side lobes present which are often found in patterns observed at single frequencies. The back lobe (which is in air) is smaller due to the shielded antenna design. As the permittivity of the dielectric environment increases from $\epsilon_r = 5$ to $\epsilon_r = 20$ the main lobes in both E- and H-plane patterns become narrower. This occurs because the critical angle becomes smaller as the permittivity increases. Energy in the critical angle window mainly comes from the spherical wave in the ground, whereas energy beyond the critical angle window is associated with lateral waves.

Maximum energy in the E-plane is directly under the antenna (180°). The H-plane patterns are asymmetric about the vertical axis (0°, 180°) because the T_x and R_x elements of the antenna are offset from each another. Consequently, maximum energy in the H-plane is offset towards the T_x element (≈150°). Fig. 4 shows a comparison of how the maximum energy decreases with observation distance for the full antenna model as well as a theoretical infinitesimal dipole model. The maximum energy at each radial distance was normalised by the maximum energy present in that set of patterns. A line showing the theoretical $\frac{1}{r^2}$ decrease in

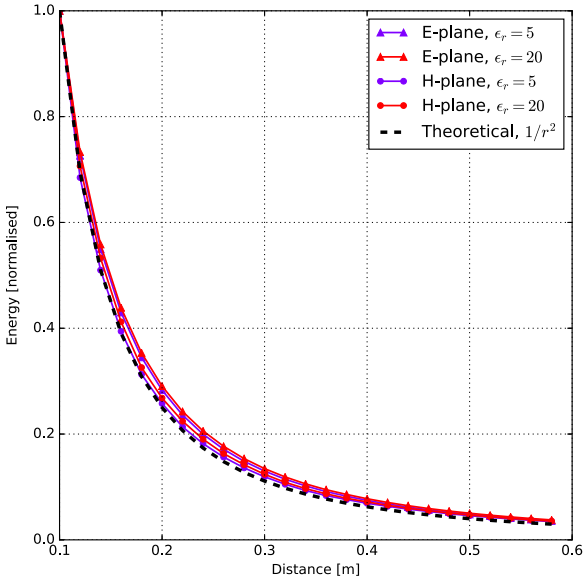

(a) Infinitesimal dipole model

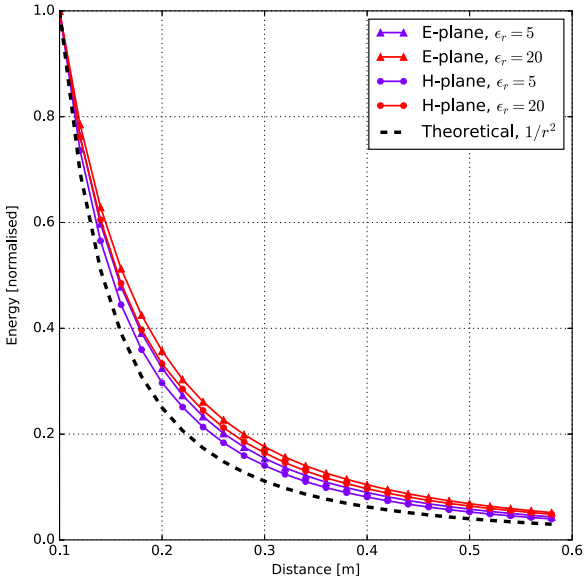

(b) Full antenna model

Fig. 4. Energy loss in dielectric half-spaces, $\epsilon_r = 5$ and $\epsilon_r = 20$, at observation distances 0.10–0.58 m at intervals of 0.02 m.

energy with observation distance (in the intermediate field region) [23] is also given. The only loss mechanism present in both simulations comes from geometric spreading of the electromagnetic waves. Both the simulation with the full antenna model and the simulation with the infinitesimal dipole follow the theoretical behaviour closely for the two dielectric environments.

The overall shape of the patterns begins to converge as the observation distance increases, which indicates the beginning of far-field behaviour. Over a lossless dielectric of relative permittivity $\epsilon_r = 5$ the theoretical transition from near-field to far-field zones (the Fraunhofer distance), based on Eq. (2), occurs at 0.0806 m. For a relative permittivity $\epsilon_r = 20$ the distance is 0.1611 m.

$$R = \frac{2D^2}{\lambda}, \tag{2}$$

where D is the largest dimension of the antenna (0.060 m), and λ is the wavelength in the medium at the centre frequency of the

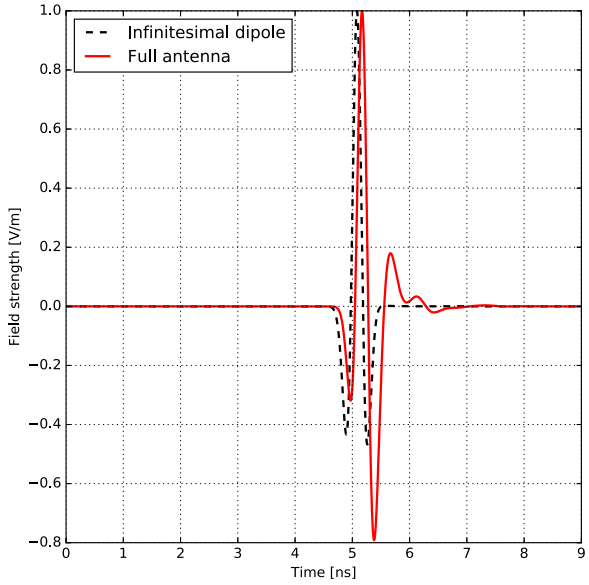

Fig. 5. Time domain responses (normalised) from the H-plane of an infinitesimal dipole model and the full antenna model at a distance of 0.58 m and an angle of 153° in a lossless dielectric environment of relative permittivity $\epsilon_r = 5$.

antenna. However, Figs. 2 and 3 clearly demonstrate that the distances at which the far-field begins are much greater than the predicted Fraunhofer distances.

The main lobes of the patterns of the infinitesimal dipole models at observation distances of 0.1 m and 0.58 m are in general agreement with those of the full antenna models. The back lobes of the patterns of the infinitesimal dipole models at observation distances of 0.1 m and 0.58 m are larger because there is no shielding structure (in fact no structure at all) present in the infinitesimal dipole models. Although the radiated energy from the infinitesimal dipole model is very similar to the full antenna model, the time-domain responses still differ. Fig. 5 shows an example of this by comparing the responses from an infinitesimal dipole model and the full antenna model in the H-plane at a distance of 0.58 m and an angle of 153° in a lossless dielectric environment of relative permittivity $\epsilon_r = 5$.

Figs. 6–8 present the principal E- and H-plane patterns in lossy heterogeneous environments with different soil properties and different fractal dimensions. The shapes of the patterns at small observation distances are quite similar to those in the dielectric environments, indicating that very close to the antenna the electric and magnetic fields are not affected by the properties of the environments. However, there are several important general differences between the patterns in the half-space dielectric environments and the heterogeneous environments. Asymmetry is now present in the shapes of the E- and H-plane patterns because of the heterogeneous nature of the environments. The shapes of the patterns are more irregular, with peaks and troughs in energy, and there is less evidence that the shapes of the patterns are converging. The heterogeneous environments are lossy, so the difference in maximum energy between observation distances of 0.01 m and 0.58 m is up to 30 dB, compared to up to 15 dB in the homogeneous dielectric half-spaces.

Again, the main lobes of the patterns of the infinitesimal dipole models at observation distances of 0.1 m and 0.58 m are in general agreement with those of the full antenna models.

Figs. 6 and 7 use the same soil properties for the lossy heterogeneous environments but with different fractal dimensions of 1.5 and 2 respectively. Increasing the fractal dimension increases the complexity of the 3D distribution of soil properties. The overall shape of the patterns with different fractal dimensions are quite

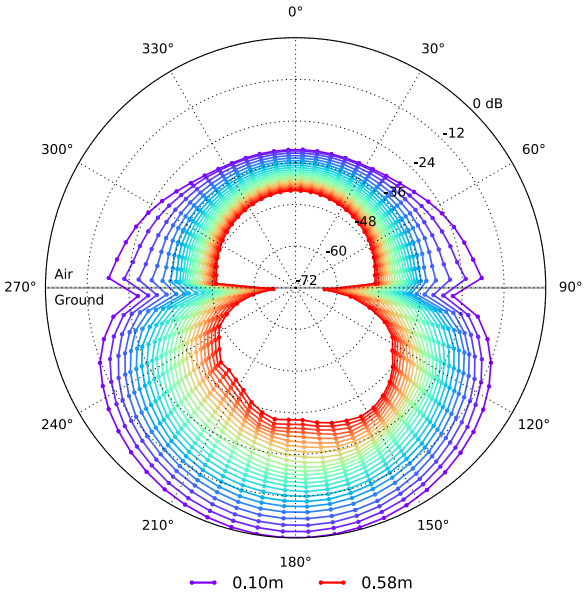

(a) E-plane

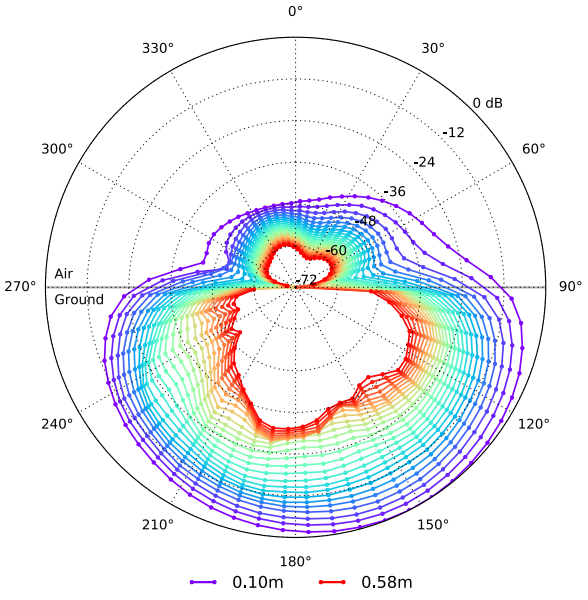

(b) H-plane

Fig. 6. Series of energy patterns from the full antenna model over a lossy heterogeneous environment with soil properties – sand fraction $S = 0.5$, clay fraction $C = 0.5$, bulk density $\rho_b = 2$ g/cm^3, and sand particle density $\rho_s = 2.66$ g/cm^3 – and a fractal dimension $D = 1.5$. Observation distances 0.10–0.58 m at intervals of 0.02 m.

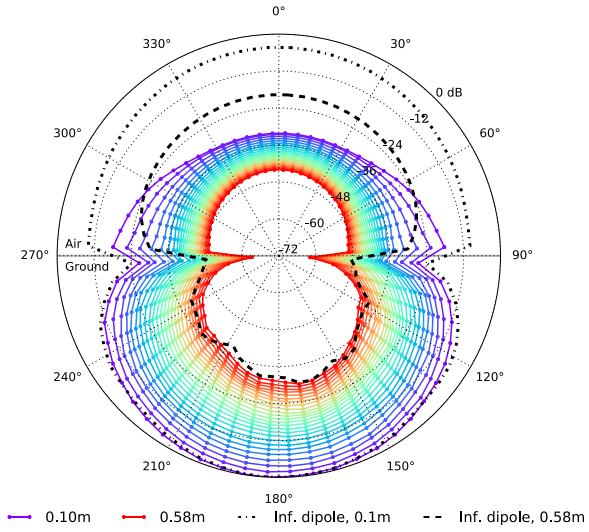

(a) E-plane

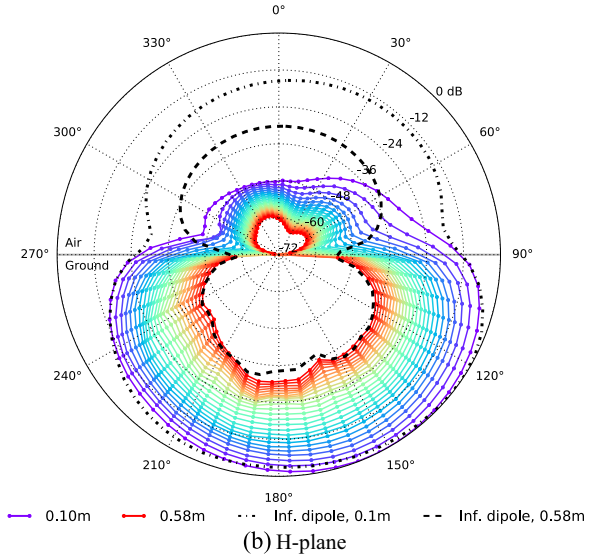

(b) H-plane

Fig. 7. Series of energy patterns from the full antenna model over a lossy heterogeneous environment with soil properties – sand fraction $S = 0.5$, clay fraction $C = 0.5$, bulk density $\rho_b = 2$ g/cm^3, and sand particle density $\rho_s = 2.66$ g/cm^3 – and a fractal dimension $D = 2$. Observation distances 0.10–0.58 m at intervals of 0.02 m. Infinitesimal dipole model over the same lossy heterogeneous environment at an observation distances of 0.1 m and 0.58 m.

similar but there are differences, especially in the shape of the H-plane patterns at observation distances greater than 0.38 m. The angle at which the maximum energy occurs does not remain consistent for observation distances greater than 0.38 m. The H-plane pattern in Fig. 6, with the smaller fractal dimension, exhibits more peaks and troughs in energy than Fig. 7 with the larger fractal dimension. This could be because the scale of the heterogeneities generated with the larger fractal dimension is very small compared to the wavelength of the central frequency of the antenna.

The final three environments investigated use the same fractal dimension of 2 but different soil properties, which represent a sandy soil ($S = 0.9$, $C = 0.1$), soil with equal sand and clay fractions ($S = 0.5$, $C = 0.5$), and a clayey soil respectively ($S = 0.1$, $C = 0.9$). Figs. 7 and 8 show that the overall shape of the main lobes of the patterns in the different soils are similar. However, in the sandy soil the main lobes are much broader, likely due to the lower permittivities present. Minimal differences were observed between the patterns in the soil with equal sand and clay fractions, and the clayey soil.

4. Conclusion

Simulations using a full antenna model of a ground-coupled, high-frequency GPR antenna over a lossless dielectric half-space provide a basic guide to how the antenna will radiate energy in more realistic environments. Despite clear differences in the individual time domain responses from the simulations that included only an infinitesimal dipole model and those that used the full antenna model, there were strong similarities in radiated energy distributions. This could be beneficial knowledge for signal

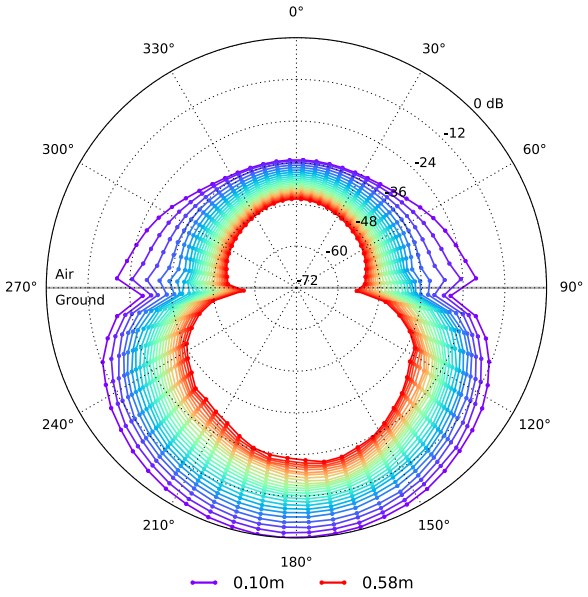

(a) E-plane

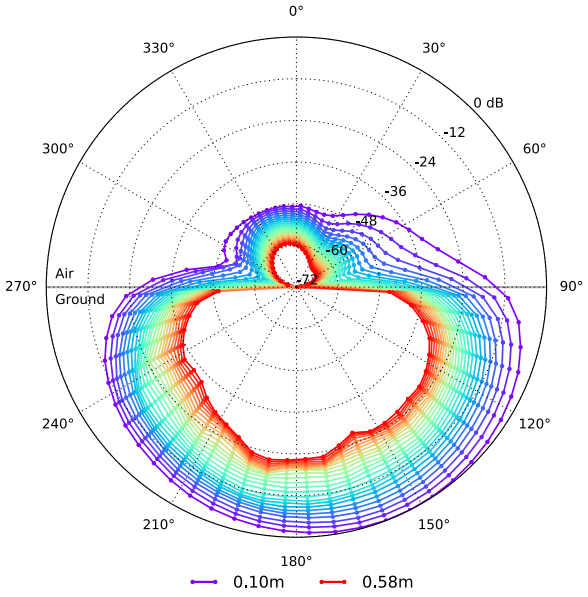

(b) H-plane

Fig. 8. Series of energy patterns from the full antenna model over a lossy heterogeneous environment with soil properties – sand fraction $S = 0.9$, clay fraction $C = 0.1$, bulk density $\rho_b = 2$ g/cm^3, and sand particle density $\rho_s = 2.66$ g/cm^3 – and a fractal dimension $D = 2$. Observation distances 0.10–0.58 m at intervals of 0.02 m.

processing and migration algorithms that assume energy distributions based on the infinitesimal dipole.

Significant variations in the magnitude and pattern shape of the radiated energy of the antenna were observed when both the infinitesimal dipole model and the full antenna model were used in the lossy heterogeneous environments. There were notable peaks and troughs in energy in both E- and H-plane patterns. These were more prominent in the H-plane which is usually the plane in which GPR surveys are performed. Again the simulations that included only an infinitesimal dipole model produced a very similar radiated energy distribution to those that used the full antenna model. Further research is being conducted to investigate the performance of the antenna in lossy heterogeneous environments that are simulated using different mixing models.

Acknowledgments

This work was supported by the Engineering and Physical Sciences Research Council (EPSRC).

References

[1] J. Van der Kruk, R. Streich, M. Grasmueck, Toward true-amplitude vector migration of gpr data using exact radiation patterns, in: Advances in Near-surface Seismology and Ground-penetrating Radar, Geophysical Developments, 2010, pp. 97–116 (Chapter 6).
[2] S. Millard, A. Shaari, J. Bungey, Field pattern characteristics of gpr antennas, NDT & E Int. 35 (7) (2002) 473–482.
[3] G. Klysz, X. Ferrieres, J. Balayssac, S. Laurens, Simulation of direct wave propagation by numerical fdtd for a gpr coupled antenna, NDT & E Int. 39 (4) (2006) 338–347.
[4] V. Pérez-Gracia, D. Di Capua, R. González-Drigo, L. Pujades, Laboratory characterization of a gpr antenna for high-resolution testing: radiation pattern and vertical resolution, NDT & E Int. 42 (4) (2009) 336–344.
[5] A. Annan, W. Waller, D. Strangway, J. Rossiter, J. Redman, R. Watts, The electromagnetic response of a low-loss, 2-layer, dielectric earth for horizontal electric dipole excitation, Geophysics 40 (2) (1975) 285–298.
[6] S. Arcone, Numerical studies of the radiation patterns of resistively loaded dipoles, J. Appl. Geophys. 33 (1–3) (1995) 39–52.
[7] C. Warren, A. Giannopoulos, Experimental and modeled performance of a ground penetrating radar antenna in lossy dielectrics, IEEE J. Sel. Top. Appl. Earth Observ. Remote Sens. 9 (1) (2015) 29–36.
[8] S. Lambot, E.C. Slob, I. van den Bosch, B. Stockbroeckx, M. Vanclooster, Modeling of ground-penetrating radar for accurate characterization of subsurface electric properties, IEEE Trans. Geosci. Remote Sens. 42 (11) (2004) 2555–2568.
[9] S. Lambot, F. André, E. Slob, H. Vereecken, Effect of antenna-medium coupling in the analysis of ground-penetrating radar data, Near Surf. Geophys. 10 (6) (2012) 631–639.
[10] N. Diamanti, A.P. Annan, Characterizing the energy distribution around gpr antennas, J. Appl. Geophys. 99 (2013) 83–90.
[11] A. Giannopoulos, Modelling ground penetrating radar by gprmax, Constr. Build. Mater. 19 (10) (2005) 755–762.
[12] N.J. Cassidy, T.M. Millington, The application of finite-difference time-domain modelling for the assessment of gpr in magnetically lossy materials, J. Appl. Geophys. 67 (4) (2009) 296–308.
[13] P. Shangguan, I.L. Al-Qadi, Calibration of fdtd simulation of gpr signal for asphalt pavement compaction monitoring, IEEE Trans. Geosci. Remote Sens. 53 (3) (2015) 1538–1548.
[14] E. Slob, M. Sato, G. Olhoeft, Surface and borehole ground-penetrating-radar developments, Geophysics 75 (5) (2010) 75A103–75A120.
[15] F. Soldovieri, J. Hugenschmidt, R. Persico, G. Leone, A linear inverse scattering algorithm for realistic gpr applications, Near Surf. Geophys. 5 (1) (2007) 29–42.
[16] M. Solla, H. Lorenzo, F. Rial, A. Novo, Ground-penetrating radar for the structural evaluation of masonry bridges: results and interpretational tools, Constr. Build. Mater. 29 (2012) 458–465.
[17] A.P. Tran, F. Andre, S. Lambot, Validation of near-field ground-penetrating radar modeling using full-wave inversion for soil moisture estimation, IEEE Trans. Geosci. Remote Sens. 52 (9) (2014) 5483–5497.
[18] Elsevier. Scopus, The Largest Abstract and Citation Database of Peer-Reviewed Literature [online, cited 2015].
[19] C. Warren, A. Giannopoulos, I. Giannakis, An advanced gpr modelling framework: the next generation of gprmax, in: 2015 8th International Workshop on Advanced Ground Penetrating Radar (IWAGPR), IEEE, Florence, Italy, 2015, pp. 1–4.
[20] C. Warren, A. Giannopoulos, Creating fdtd models of commercial gpr antennas using Taguchi's optimisation method, Geophysics 76 (37) (2011) G37–G47.
[21] M.C. Dobson, F.T. Ulaby, M.T. Hallikainen, M.A. El-Rayes, Microwave dielectric behavior of wet soil – Part II: Dielectric mixing models, IEEE Trans. Geosci. Remote Sens. 23 (1) (1985) 35–46.
[22] I. Giannakis, A. Giannopoulos, A novel piecewise linear recursive convolution approach for dispersive media using the finite-difference time-domain method, IEEE Trans. Antennas Propag. 62 (5) (2014) 2669–2678.
[23] C. Balanis, Antenna Theory: Analysis and Design, 2nd edition, John Wiley and Sons, Inc., Canada, 1997.